THE COUNTER–CURRENT FLOODING LIMIT IN VERTICAL TUBES WITH AND WITHOUT ORIFICES

P. Tye,[1] *M. Davidson,*[1] *A. Teyssedou,*[1]
A. Tapucu,[1] *A. Matuszkiewicz,*[1] and *W. Midvidy*[2]

(1) Institut de Génie Énergétique
École Polytechnique de Montréal
Montréal, Québec, Canada H3C 3A7
(2) Ontario Hydro

ABSTRACT

For hypothetical loss of coolant accidents in nuclear reactors, rapid reflooding of the core is desirable. In CANDU reactors the cooling water is injected into the headers which are connected to the fuel channels by the feeder pipes. These pipes consist of vertical and horizontal runs; in some feeders, orifices and/or venturi flow meters are installed for flow adjustments and measurements respectively. For certain postulated accident scenarios, steam coming from the fuel channels and/or generated in the hot feeders may flow in the direction opposite to that of the cooling water thereby, creating a vertical or horizontal counter–current two–phase flow. Under these conditions, the rate at which cooling water can enter the fuel channels may be limited by the flooding phenomena. This phenomena is greatly affected by the geometry of the feeder pipes, shape and number of fittings, and the flow area restrictions located in the feeders.

In this paper the influence that orifice type flow area restrictions have on the counter–current flooding limit (CCFL) in a vertical tube is examined. Air and water at close to atmospheric conditions are used as the working fluids. The data collected on the counter–current flooding limit in a vertical tube both with and without flow area restrictions is compared against some of the most commonly used correlations that are available in the open literature. Data on the two–phase counter–current pressure drop below the flooding point are also presented.

Paper submitted to The Canadian Nuclear Society 4th International Conference on Simulation Methods In Nuclear Engineering

1. INTRODUCTION

Counter–Current Flow (CCF) in general and the Counter–Current Flooding Limit (CCFL) in particular are of great importance in the area of nuclear reactor safety analysis. In CANDU reactors, during a postulated loss of coolant accident, the cooling water coming from the inlet and outlet headers enters the fuel channels through feeder pipes. These pipes consist of vertical and horizontal runs; in some feeders, orifices and/or venturi flow meters are installed for flow adjustments and measurements. Steam generated in the fuel channel and/or in the hot feeders may flow in the direction opposite to that of the cooling water thereby, creating a vertical or horizontal counter–current two–phase flow. Under these conditions, the rate at which water can enter the fuel channels may be limited by the flooding phenomena. At the flooding point, the liquid is partly entrained in the same direction as the steam flow. This point is greatly affected by the geometry of the feeder pipes, shape and number of fittings, and flow area restrictions located in the feeders.

In this paper the influence that orifice type flow area restrictions have on the counter–current flooding limit (CCFL) in a vertical tube is examined. The data collected on the counter–current flooding limit in a vertical tube both with and without flow area restrictions is compared against some of the most commonly used correlations that are available in the open literature. Data on the two–phase counter–current pressure drop below the flooding point is also presented.

2. COUNTER–CURRENT TWO–PHASE FLOW TEST FACILITY

The CCF test facility consists of a $\simeq 3.0\ m$ vertical test section made of a 19 mm I.D. transparent plexiglass tube to allow flow visualization. The test section is mounted on an I–beam aluminum structure and is positioned vertically by using 4 adjustable supports. Water and air at atmospheric pressure conditions are used as the working fluids. The water is supplied to the test section by a pump connected to a constant head water tank. Coarse and fine water flow rate adjustments are done by means of a set of valves. The water flow rate at the inlet of the test section is measured with a bank of "Flow Technology" flow meters covering a range of 0.015 to 1.00 l/s. According to the manufacturer the accuracy of these meters is better than 1% of the readings. The temperature of the inlet water is kept almost constant at $20.0\pm0.5°C$. The air is supplied by the mains of the laboratory. The air flow rate is measured with a bank of five "Brooks" rotameters, covering the range of 0.02 to 40.0 l/s. The rotameters have been calibrated to an accuracy of 1% of full scale. The temperature of the air is continuously monitored with a thermocouple installed in the air flow line and has a value of $23\pm1°C$.

A schematic diagram of the test facility is shown in the Figure 1. Two different liquid injection methods are used during the experiments: a porous wall type injector and an overflow type injector. In the first case, the liquid is injected into the test section through four hundred 1 mm holes drilled in the wall of a bronze tube which has the same I.D. as the test section. This system allows a uniform annular liquid film to be formed inside the test section. In the second method, the liquid film is formed by an overflow type injector placed at the entrance of the test section in the upper plenum. The inlet of this injector has a similar geometry to that of the feeder–header connection in CANDU reactors. Besides the overflow injector, a separator used to collect entrained droplets has also been installed in the upper plenum.

For the pressure drop experiments two different air injection systems are used. The first consists of a laminar flow straightener and a nozzle which is aligned with the test section and is installed in the lower plenum (Figure 2). In the second method air is injected directly into the lower plenum (Figure 2). For the flooding experiments only the nozzle aligned with the test section was used for

the air injection. The lower plenum also collects and evacuates the liquid from the falling film.

The test section is instrumented to measure the absolute pressure in the lower plenum and the total pressure drop in the liquid film over eleven 200 *mm* intervals along the tube. To the best of our knowledge these are the first measurements of the total pressure drop in the liquid film taken with this much detail over the entire lenght of the test section for counter–current flows. Other authors (i.e., Dukler & Smith [1979], Bharathan *et. al.* [1979] and Zabaras [1985]) limited their pressure measurements to only one interval. The absolute pressure is measured with a 0.14 *bar* dry leg "Sensotec" pressure transducer with an accuracy of ±0.25% of full scale. The axial pressure drop is measured with 0.035 *bar* wet legs "Sensotec" pressure transducer with an accuracy of ±0.25% of full scale. In order to get a better idea on the average pressure prevailing in the test section, at a given axial location, there are three pressure taps on the wall of the tube separated by 120°. These taps are connected to the pressure transducers through pressure collars as illustrated in Figure 2. The output of the absolute pressure transducer is continuously recorded for CCFL detection.

3. EXPERIMENTAL PROCEDURE

The objectives to this research program are two–fold, first to study the effect of flow area restrictions on the CCFL and second to obtain detailed information on the axial pressure variation in counter–current two–phase flows.

For the counter–current flooding limit experiments, different flow area restrictions (orifice) were installed in the test section 2123 *mm* below the upper plenum. The orifices were made of bronze plates without a chamfered edge and having a thickness of 1.5 *mm*. Four orifices having β ratios ($\beta = D_{orifice}/D_{tube}$) of 0.90, 0.83, 0.72, and 0.66 were used. In these experiments the liquid flow rate was fixed and the gas flow rate was gradually increased until the flooding point was reached. This point was detected by monitoring the pressure in the lower plenum and determining the gas flow rate at which a substantial increase in this pressure was observed. As described by Tien & Liu [1979], three criteria have been used for the characterization of CCFL by different authors:

a) zero liquid penetration,

b) inception of liquid film upflow, and

c) point of inception of liquid entrainment.

However, for a given liquid flow rate these events occur at significantly different gas flow rates. Thus, it is obvious that a lack of clarity and consistency in the definition used will significantly affect the flooding data. Therefore, in this work the definition of flooding given by Bankoff & Lee [1986] is used as the experimental criterion to determine the flooding point That is: *"for a given downward liquid flow the maximum upward gas flow rate for which full liquid delivery out the bottom of the tube is maintained, corresponds to the counter–current flooding limit."* this is the most widely accepted experimental criterion for the point of flooding (Dukler *et. al.* [1984] and Bankoff & Lee [1986]). In the absence of net entrainment as is the case for the small diameter and long test section used for these experiments, this point corresponds to the point of inception of liquid film upflow (criterion b). It also corresponds to the jump of the absolute pressure in the lower plenum.

The pressure drop experiments were carried out for the range of water flow rates from 0.05 to 0.24 m^3/h and a range of gas flow rates from 0.0 to 4.08 m^3/h; for a given liquid flow rate the widest possible range of gas flow rates below the flooding point was covered. The experiments were conducted with both gas injection methods. No pressure drop data were collected at the flooding point. The variation of the pressure drop in the test section is determined by adding up

the eleven ΔP measurements resulting from the 12 pressure measurement stations. The actual distance between each station has been measured with a digital caliper to the nearest 0.01 mm. The lines connecting all the pressure taps to the pressure transducers are water filled. The pressure drop measurements are taken between two successive pressure taps and are then corrected for the water head of the pressure lines. The schematic of the pressure measurement system is shown in Figure 2.

Details regarding the procedure used to measure the axial pressure drop are illustrated using Figure 3. To eliminate any systematic errors due to the electronic drift of the pressure transducers and the hydraulic head introduced by the pressure lines, the axial pressure drop is determined in the following manner:

1. the pressure is first measured with the upstream (with respect to the water flow direction) pressure collar connected to the negative side of the pressure transducer and the downstream pressure collar connected to the positive side of the pressure transducer (P_2 and P_1 in Figure 3),
2. next the pressure is measured with the downstream (with respect to the water flow direction) collar connected to the negative side of the pressure transducer and the upstream pressure collar connected to the positive side of the pressure transducer (P_2' and P_1' in Figure 3),
3. to obtain the actual pressure difference between two succesive pressure taps the results of these two measurements are then averaged and corrected for the hydrostatic head in the measurement line using the following equation:

$$\overline{P_2 - P_1} = -\frac{\Delta P_m - \Delta P_m'}{2} - g\rho_f \Delta h \quad , \tag{1}$$

where:

$$\Delta P_m = -P_2 + P_1 \quad , \tag{2}$$

and

$$\Delta P_m' = P_2' - P_1' \quad . \tag{3}$$

The pressures used in the above equations result from the average of ten readings each of which is the result of the average signals generated by the differential pressure transducer and collected during a 10 second interval using a "Fluke" programmable digital voltmeter with a sampling time of 1 ms.

4. EXPERIMENTAL RESULTS

Figure 4 shows the data obtained on counter–current flooding limit using both liquid injection methods (porous wall and overflow) on the test section with and without orifices. The flooding data is presented in terms of the square root of the non dimensional superficial velocies, $J_g^{*\frac{1}{2}}$ and $J_f^{*\frac{1}{2}}$. It is of great importance to first examine the behaviour of the CCFL for a given test facility due to the fact that this limit is substantially affected by the entrance and exit geometry of the test section. For this reason, the CCFL experiments were conducted in two series. The first series of experiments were carried out on a test section without an orifice using both injection methods. The widest possible range of flow parameters (liquid and gas flow rates) were used in the experiments.

As can be observed from Figure 4, at least for this series of experiments, for values of $J_f^{*\frac{1}{2}} < 0.6$ the flooding limit does not seem to be influenced appreciably by the liquid injection method. For liquid flow rates larger than $J_f^{*\frac{1}{2}} = 0.6$ the liquid injection method does influence the flooding limit. Above $J_f^{*\frac{1}{2}} = 0.6$ the flooding data collected using the porous wall liquid injector shows a change in the slope of its distribution.

The second series of experiments were conducted on a test section with different orifices installed in it using both injection methods. Again the widest possible range of liquid and gas flow rates for each given orifice have been covered during these experiments. Figure 4 also shows the data obtained with the different orifices installed in the test section. Visual observation has shown that for the cases involving an orifice the flooding always occured at the orifice. Below the flooding point the effect of the orifice was to cause the liquid to be redirected towards the center of the tube, 4 or 5 cm below the orifice the liquid film flowing on the tube wall was seen to re–establish itself. As was observed in the experiments without an orifice, there seems to be little affect of the injection method below a threshold value at which point the slope of the distribution of the observed flooding points using the porous wall injector begins to drop as was observed in the experiments without the orifice. The presence of the orifice significantly reduces the gas flow rate required to initiate flooding for a given liquid flow rate. Further, it can also be seen that the flooding limit is greatly affected by the β ratio of the orifice.

Figures 5 and 6 show typical results of the pressure drop profiles measured in the liquid film obtained for a water flow rate of 0.1 m^3/h and a number of different gas flow rates. It is observed that the pressure decreases almost linearly in the liquid flow direction. Figure 5 shows the pressure drop profile when the gas is injected using the gas injector and Figure 6 shows the pressure drop profile when the gas is injected from the top of the lower plenum. The comparison of these figures shows that there is almost no influence of the gas injection method on the total pressure drop. However the use of the gas injector makes it possible to go to higher gas flow rates and still remain below the flooding point.

One of the most important features of the results presented in Figures 5–7 is that the pressure measured in the liquid film decreases in the downward direction for all gas and liquid flow rates. The reason for such an axial profile of the film pressure as that found in our experiments is not clear. For a vertical counter–current flow it is expected that the gas pressure will decrease in the upward direction. It is difficult to understand how the gas and liquid pressure are balanced at a given cross–sectional plane. However, Biage [1989] reported that for some of his runs the gas pressure decreased in the downward direction. He tried to explain this by the entrainment of the liquid droplets. The results reported in this paper and those of Biage [1989] indicate that a commonly adopted assumption in two–phase flow modeling, that the gas and liquid pressures are equal, might not hold for counter–current flows.

If one supposes that the liquid film pressure decreases in the downward direction as suggested by our data it is not difficult to understand the other features of the results presented in Figures 5–7. Our data shows that the pressure drop in the liquid film decreases with increasing gas flow rates. This may be due to the net effect of an increase in the upwardly directed interfacial friction and the decrease in the upwardly directed wall shear stress, that is caused by the gas flow on the liquid film (Zabaras [1985] and Matuszkiewicz *et. al.* [1993]). Figure 7 shows the total pressure drop across the test section well below the flooding point for a number of different gas flow rates with increasing liquid flow. It can be observed that for a given gas flow rate the total pressure drop decreases with an increasing liquid flow rate. This fact may be partially related to some entrance effects due to the gas injection. However, the same behaviour has been observed in experiments

that have been carried out with zero gas flow rate and the lower plenum completely open to the atmosphere. These results are shown in Figure 8 and confirm that even in the absence of the gas entrance effects the total pressure drop in the liquid film decreases with increasing liquid flow rate.

5. COMPARISON BETWEEN EXPERIMENTAL RESULTS AND FLOODING CORRELATIONS

The data on the CCFL without orifices are compared to the most commonly used flooding correlations; these are: a modified form of the empirical correlation due to Alekseev (McQuillan & Whalley [1985]), the theoretical correlation due to Bharathan *et. al.* [1978], the most common correlation in the literature due to Wallis [1969]. The data on the CCFL with orifices are compared to the correlation of Celata *et. al.* [1989] which takes into account the effect of the flow area restrictions.

i) Alekseev Flooding Correlation

According to McQuillan & Whalley (1985) the most successful correlation that they tested was a modified form of the Alekseev correlation. This correlation is given by:

$$K_g = 0.286 Bo^{0.26} Fr^{-0.22} \left\{ 1 + \frac{\mu_f}{\mu_w} \right\}^{-0.18} , \tag{4}$$

where μ_f is the viscosity of the liquid under consideration, and μ_w is the viscosity of water. K_g is the gas Kutateladze number which for the k^{th} phase is given by:

$$K_k = \frac{J_k \rho_k^{1/2}}{\left[g\sigma \left(\rho_f - \rho_g \right) \right]^{1/4}} , \tag{5}$$

Bo is the Bond number given by:

$$Bo = \left[\frac{D^2 g \left(\rho_f - \rho_g \right)}{\sigma} \right] , \tag{6}$$

and Fr is the Froude number given by:

$$Fr = \frac{Q_f}{P_w} \left[\frac{g \left(\rho_f - \rho_g \right)^3}{\sigma^3} \right]^{1/4} . \tag{7}$$

ii) Bharathan Flooding Correlation

This theoretical flooding correlation was developed by Bharathan *et. al.* [1978] assuming an infinitly long tube and negligeable end effects. It yields a theoretical "upper limit" to the continued existance of counter-current flow; it is given by:

$$\frac{2 f_w J_f^{*2}}{(1-\alpha)^2} + \frac{2 f_i J_g^{*2}}{\alpha^{2.5}} = (1-\alpha) , \tag{8}$$

where the wall and interfacial friction factors are $f_w = 0.005$, and $f_i = f_w + 14.6\,(1-\alpha)^{1.87}$, respectively. In this paper, as in the work of McQuillan & Whalley [1985], the above correlation was modified to yield the square root of the non dimensional superficial gas velocity for flooding. The modified form is obtained by using the definition of the superficial liquid velocity corresponding to a liquid mass flow rate M_f (kg/s):

$$J_f = \frac{4\,M_f}{\rho_f \pi D^2}\ , \tag{9}$$

and the superficial liquid Reynolds number defined as:

$$Re_{sf} = \frac{\rho_f\, J_f D}{\mu_f}\ . \tag{10}$$

The Reynolds number is then used to calculate the mean non dimensional film thickness which is given $\delta^* = 0.908 Re_{sf}^{0.333}$ for a laminar film, i.e., Re_{sf} less than 2064, and by $\delta^* = 0.135 Re_{sf}^{0.583}$ for a turbulent film, i.e., Re_{sf} greater than or equal to 2064. Using the non dimensional film thickness, δ^*, the actual film thickness, δ, is calculated using:

$$\delta^* = \delta \left(\frac{g\rho_f\,(\rho_f - \rho_g)}{\mu_f^2} \right)^{\frac{1}{3}}\ , \tag{11}$$

and the corresponding void fraction, α, is given by:

$$\alpha = \left(1 - \frac{2\delta}{D}\right)^2\ . \tag{12}$$

Knowing the void fraction and the non dimensional liquid superficial velocity, the square root of the non dimensional gas superficial velocity corresponding to the flooding point is then calculated from:

$$J_g^{*\frac{1}{2}} = \left\{ \left[(1-\alpha) - \frac{2 f_w\, J_f^{*2}}{(1-\alpha)^2} \right] \frac{\alpha^{2.5}}{2 f_i} \right\}^{\frac{1}{4}}\ . \tag{13}$$

iii) Wallis Flooding Correlation

Wallis' flooding correlation (Wallis [1969]) is given by:

$$J_g^{*\frac{1}{2}} + m J_f^{*\frac{1}{2}} = C\ , \tag{14}$$

where m is between 0.8 and 1.0, and C is between 0.7 and 1.0. The Wallis parameter, $J_k^{*\frac{1}{2}}$, is defined as:

$$J_k^{*\frac{1}{2}} = \left\{ \frac{\rho_k^{\frac{1}{2}} J_k}{[gD(\rho_f - \rho_g)]^{\frac{1}{2}}} \right\}^{\frac{1}{2}}\ . \tag{15}$$

iv) Celata *et. al.* Flooding Correlation

The correlation of Celata *et. al.* [1989], developed to account for an obstruction in the channel, is simply Wallis' flooding correlation written under the following form:

$$J_{go}^{*\frac{1}{2}} + J_{fo}^{*\frac{1}{2}} = C_0 \gamma^{0.35} \ . \tag{16}$$

In the above correlation $C_0 = 1.0$ and γ is the perforation ratio defined as:

$$\gamma = \frac{A_{orifice}}{A_{tube}} \ , \tag{17}$$

and γ is related to β as: $\gamma = \beta^2$. *It is important to note that for this correlation the superficial velocities are calculated using the orifice diameter.*

5.1 Comparisons with Experimental Data

Figure 9 shows the comparison between the experimental flooding data for the cases without an orifice and the results of the Alekseev (Eq. 4), Bharathan (Eq. 13), and Wallis (Eq. 14) flooding correlations. McQuillan & Whalley [1985], claimed that the best overall correlation was that of Alekseev. However, their data base included a number of flooding points for which the working fluid was not necessarily water, this is taken into account by the Alekseev correlation but not by the Wallis correlation. It can be seen, that the Wallis correlation with $m = 1$ and $C = 1$ yields the best results over the entire range of $J_g^{*\frac{1}{2}}$ covered. However, for values of this variable lower than 0.3 this correlation is not very accurate. This fact may be related to the substantial change of the slope observed in the distribution of the experimental data at large liquid flow rates for the porous wall liquid injector. Further, it may also be seen that the Alekseev and Bharathan correlations do not follow the experimental trends.

Figure 10 shows the comparison between flooding data obtained with different orifices installed in the test section and the Celata *et al.* correlation (Eq. 16). It can be seen that the use of orifice diameter in the calculation of the non–dimensional superficial velocities tends to cause the data to be grouped about a given line. Table 1 shows the RMS error for the Celata *et al.* correlation compared to the experimental data for the four orifices used in these experiemnts. Within the accuracy of the experimental data the average RMS errors are on the order of about 51% and that the errors in the predicted values are independent of the orifice β. It is clear that in order to better predict the counter–current flooding limit in tubes containing orifices it will be necessary to significantly improve the available correlations, or develop a new correlation based on a larger data base.

Table 1

RMS Error of the Celata Correlation V.S. Experimental Data

Orifice β	RMS ERROR (%)	
	Injector	Overflow
0.66	43.43	64.98
0.72	38.98	59.94
0.83	53.80	56.04
0.90	37.91	51.50

6. CONCLUSIONS

Experimental data on pressure drop in counter–current two–phase flow and on the flooding limit has been presented. For these experiments air and water at close to atmospheric pressure have been used as the working fluid. The pressure drop behaves almost linearly and follows the liquid film flow. Two different liquid injection methods have been used for the CCFL experiments it was found that for high liquid flow rates the porous wall liquid injection method lead to flooding at lower gas flow rates than the overflow injector. These experiments were repeated with an orifice installed in the test section, showing that the CCFL is significantly reduced by the presence of the flow restriction. Work is underway to repeat the same experiments in a vertical tube with a 63.5 mm I.D. tube.

The comparisons of the CCFL data without the orifice with empirical and theoretical correlations show that the Wallis correlation yields the best results. The data on CCFL with an orifice are not particularly well predicted by the Celata *et al.* correlation.

ACKNOWLEDGEMENTS

This work has been funded by COG (CANDU Owners Group) under contract number WPIR 1513, Safety and Thermalhydraulics, Working Party #5.

REFERENCES

BANKOFF S.G. & LEE S.C. [1986] " A Critical Review of the Flooding Literature." *In:* Multiphase Science and Technology (G.F. Hewitt, J.M. Delaye and N. Zuber, *Eds.*). Hemisphere Publishing Co., N.Y., Vol. 2, Chapter 2.

BHARATHAN D., G.B WALLIS & RICHTER H.J. [1978] "Air–water Countercurrent Annular Flow in Vertical Tubes." EPRI Report No. EPRI NP–786.

BHARATHAN D., G.B WALLIS & RICHTER H.J. [1979] "Air–water Countercurrent Annular Flow." EPRI Report No. EPRI NP–1165.

BIAGE, M. [1989] "Structure de la Surface Libre d'un Film Liquide Ruisselant sur une Plaque Plane Verticale et Soumis a un Contre–Courant de Gaz: Transition Vers L'Écoulement Co-Courant Ascendant." Ph.D. Thesis Institut National Polytechnique de Grenoble, France.

CELATA G.P., N. CUMO G.E., FARELLO & SETARO T. [1989] "The Influence of Flow Obstructions on the Flooding Phenomenon in Vertical Channels." Int. J. Multiphase Flow, Vol. 15, No. 2, pp. 227–239.

DUKLER A.E. & L. SMITH [1979] "Two–Phase Interactions in Countercurrent Flow: Studies of the Flooding Mechansism." NUREG/CR–0617.

DUKLER A.E., L. SMITH & CHOPRA A. [1984] "Flooding and Upward Film Flow in Tubes–I." Int. J. Multiphase Flow, Vol. 10, No. 5, pp. 585–597.

MATUSZKIEWICZ A., TEYSSEDOU A. and TAPUCU A., [1993] "Modeling of the Frictional Terms for Counter–Current Gas–Liquid Flow." Submitted to the 29^{th} National Heat Transfer Conference, Atlanta.

McQUILLAN K.W. & WHALLEY P.B. [1985] "A Comparison Between Flooding Correlations and Experimental Flooding Data for Gas–Liquid Flow in Vertical Circular Tubes." Chem. Engng. Science, Vol. 40, No. 8, pp. 1425–1440.

TIEN C.L. & LIU C.P., [1979] "Survey on Vertical Two–Phase Counter–Current Flooding", Report No. EPRI NP–984.

WALLIS, G.B. [1969] "One–dimensional Two–Phase Flow." McGraw Hill, N.Y.

ZABARAS, G. [1985] "Studies of Vertical Annular Gas–Liquid Flows." Ph.D. Thesis, University of Houston, U.S.A..

NOMENCLATURE

A	Cross sectional area (m^2).
Bo	Bond number.
D	Diameter (m).
f	Friction factor.
Fr	Froude number.
g	Gravitational acceleration (m/s^2).
J	Superficial Velocity (m/s).
J_o	Superficial Velocity Calculated with the Orifice Diameter (m/s).
K	Kutateladze number.
M	Mass flow rate (kg/s).
P	Pressure (Pa).
P_m	Measured Pressure (Pa).
P_w	Wetted perimeter (m).
Q	Volumetric flow rate (m^3/s).
Re_{sf}	Liquid Superficial Reynolds number.
α	Void Fraction.
β	Orifice ratio $(= D_{orifice}/D_{tube})$.
δ	Liquid film thickness (m).
δ^*	Non dimensional liquid film thickness.
γ	Perforation Ratio $A_{orifice}/A_{tube}$.
ρ	Density (kg/m^3).
σ	Surface Tension (N/m).
μ	Viscosity $(N\,s/m^2)$.

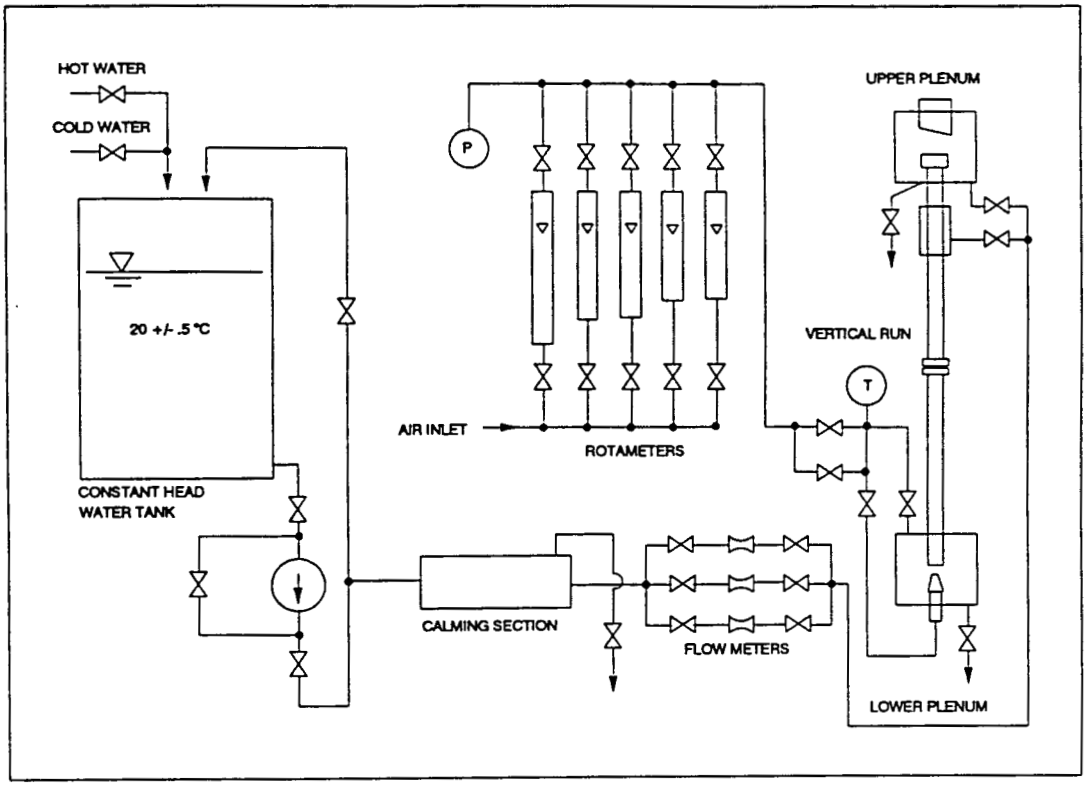

FIGURE 1. Experimental Facility.

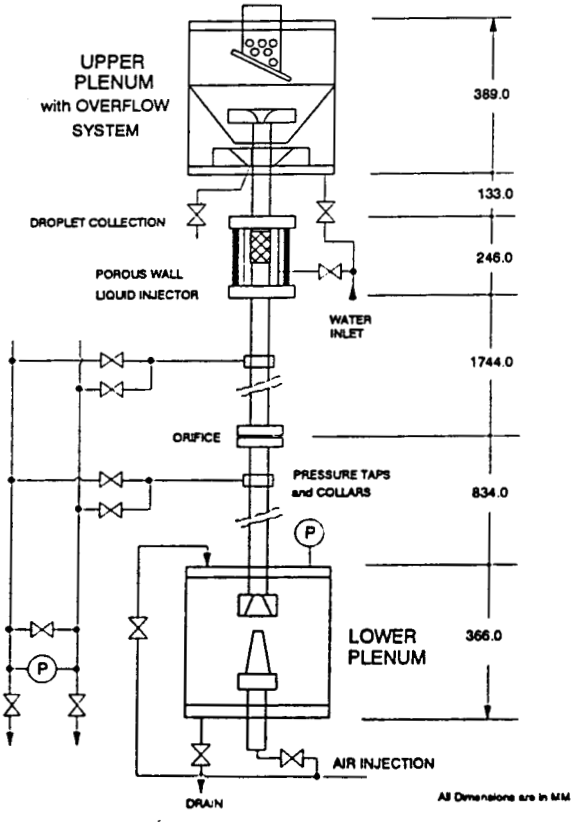

FIGURE 2. Test Section.

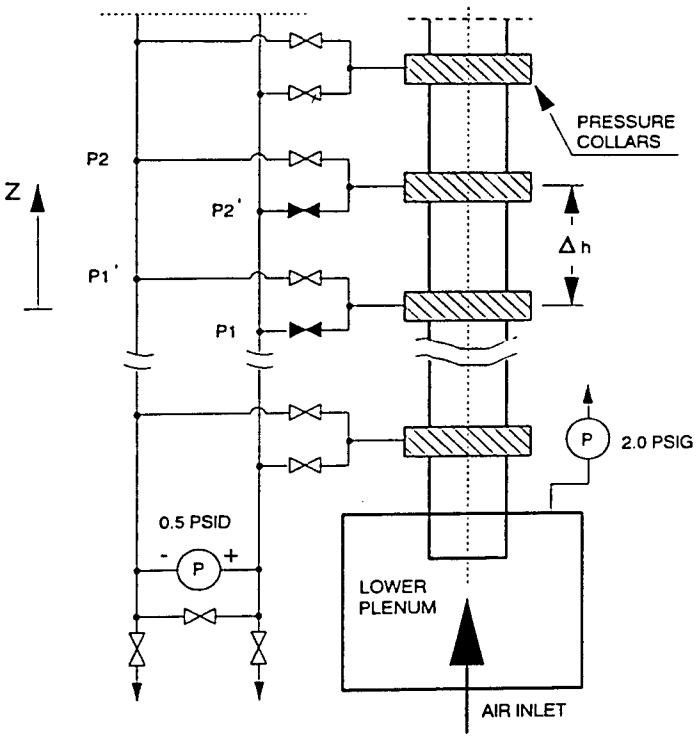

FIGURE 3. Pressure Measurement System.

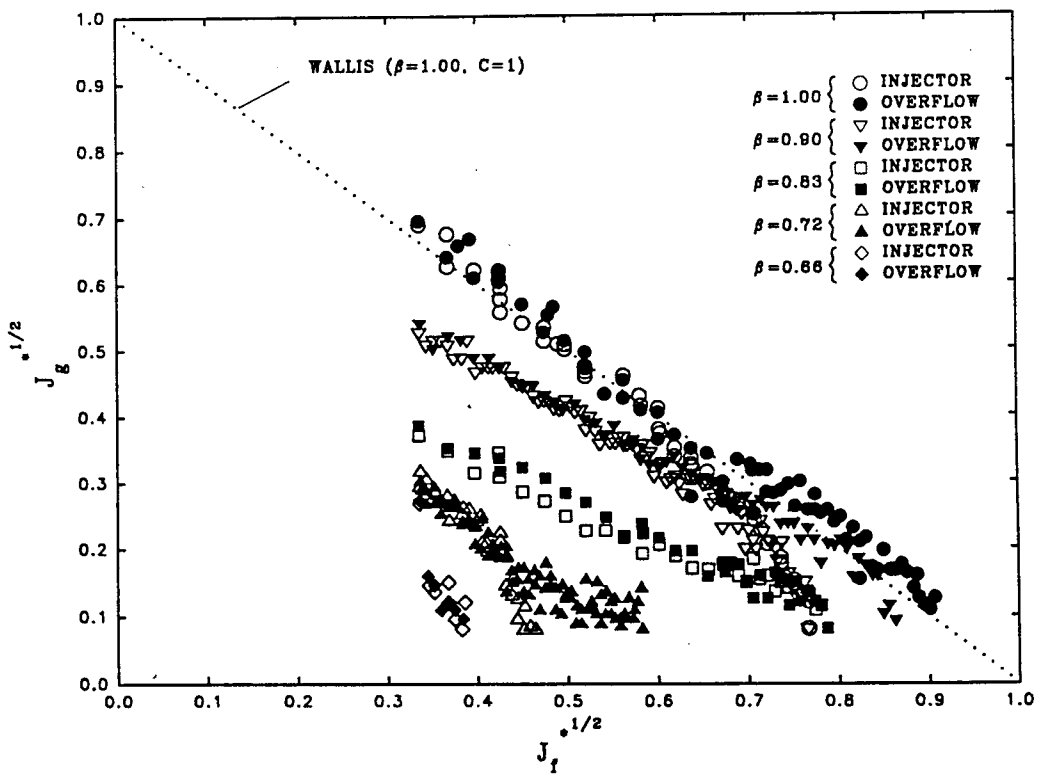

FIGURE 4. Flooding Data with and without Orifice.

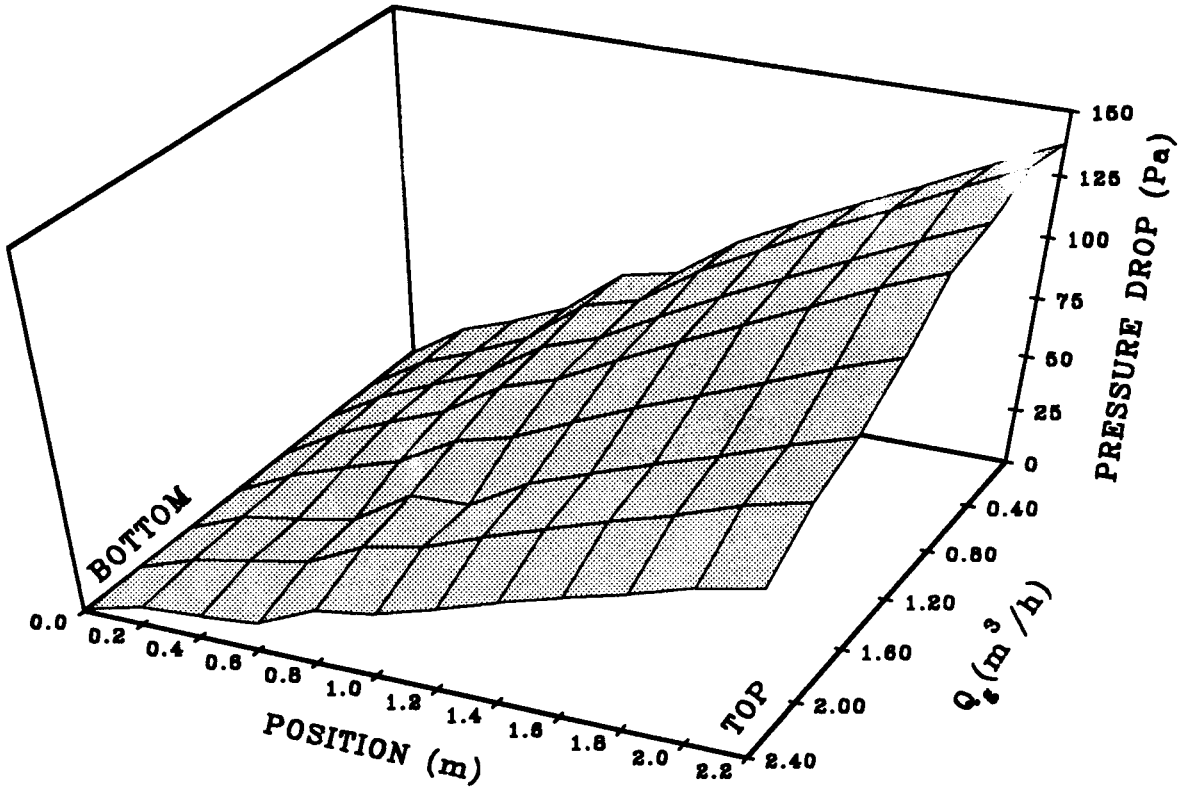

FIGURE 5. Pressure Drop vs. Gas Flow Rate (Air Injector).

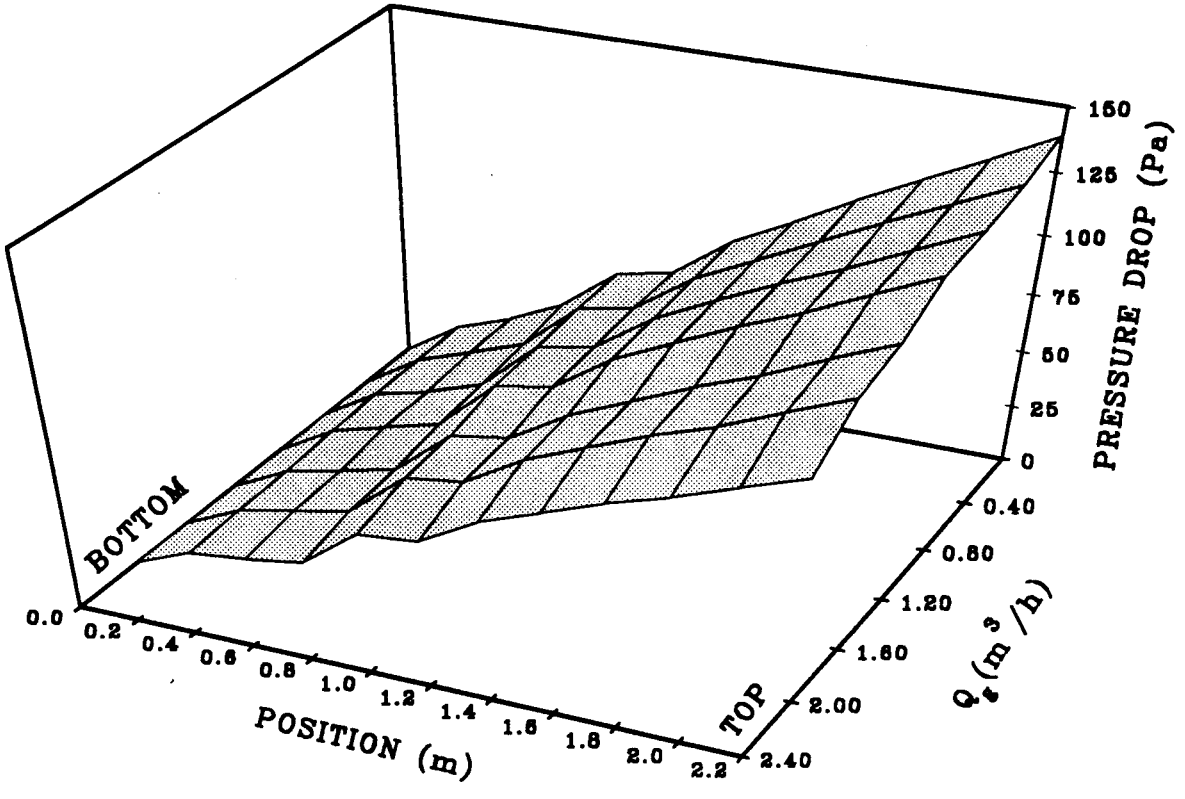

FIGURE 6. Pressure Drop vs. Gas Flow Rate (Air Injected Into Lower Plenum).

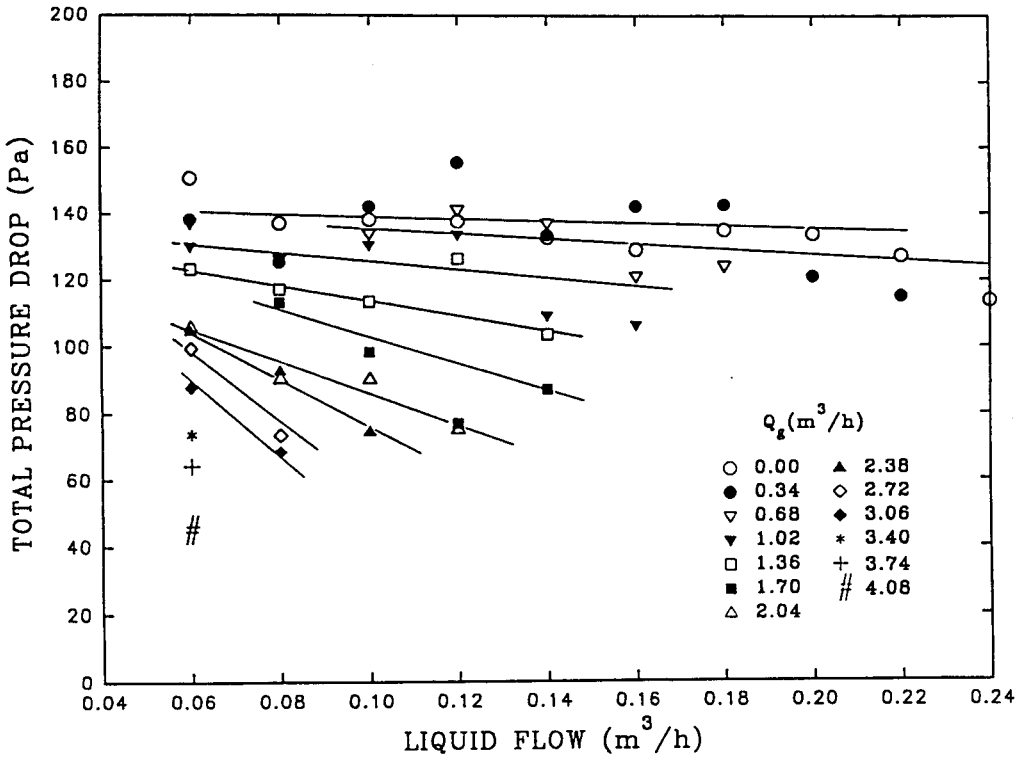

FIGURE 7. Total Pressure Drop vs. Liquid Flow Rate.

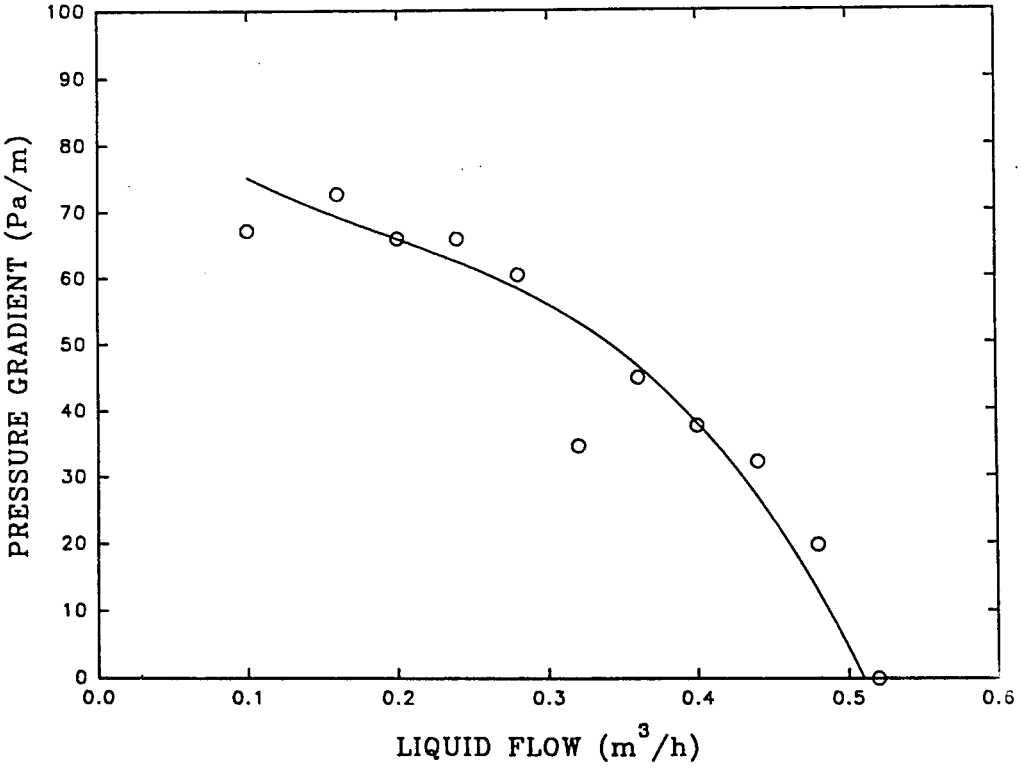

FIGURE 8. Pressure Gradient vs. Liquid Flow Rate.

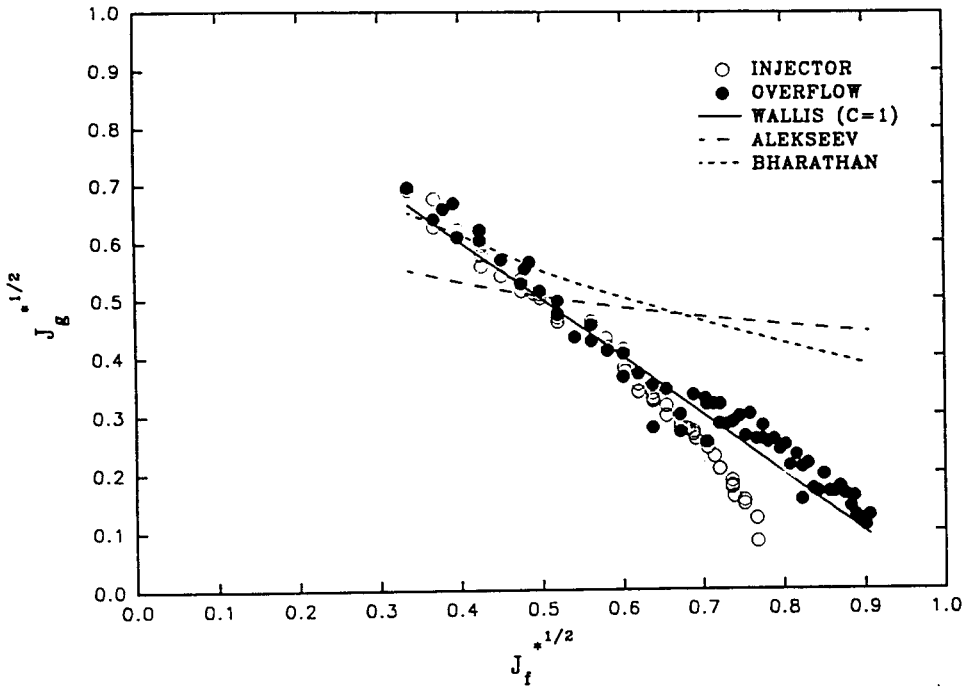

FIGURE 9. Comparison of Experimental Flooding Data without Orifice and Correlations.

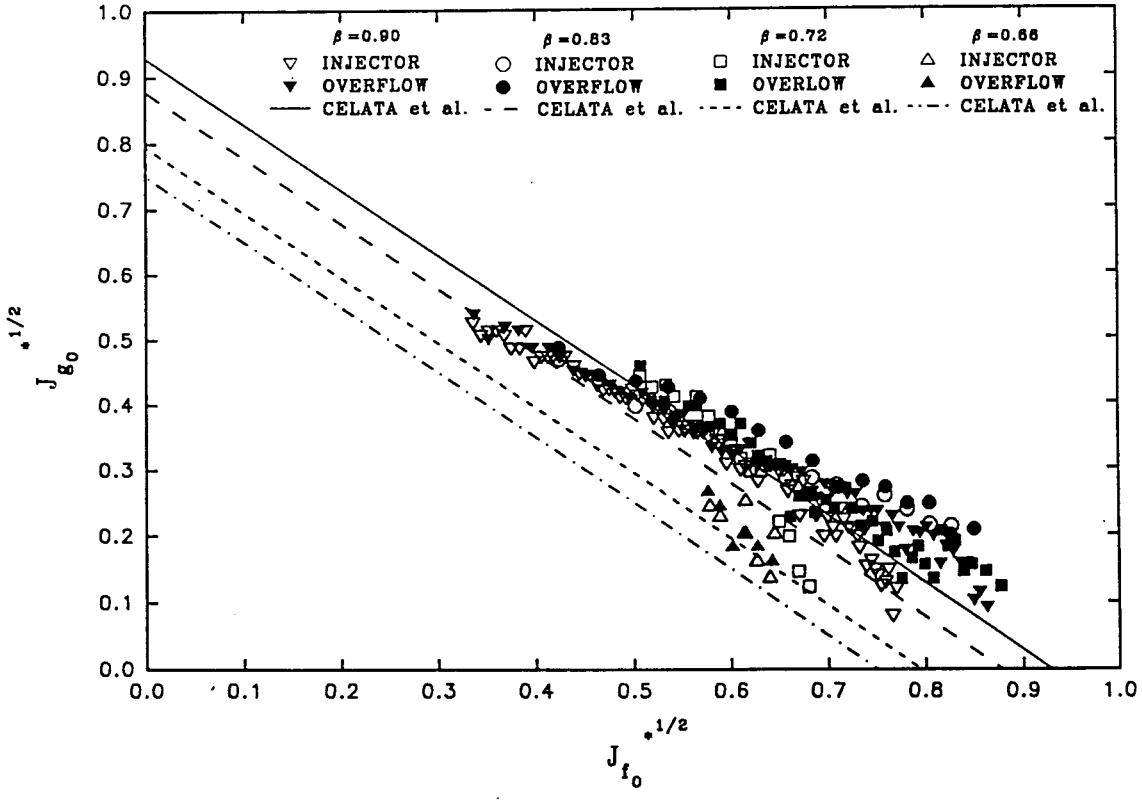

FIGURE 10. Comparison of Experimental Flooding Data with Orifices and Correlations.